Phosphorylation of a constitutive serine inhibits BK channel variants containing the alternate exon "SRKR"

Chris Shelley, Joshua P. Whitt, Jenna R. Montgomery, and Andrea L. Meredith

Department of Physiology, University of Maryland School of Medicine, Baltimore, MD, 21201

BK Ca^{2+}-activated K^+ currents exhibit diverse properties across tissues. The functional variation in voltage- and Ca^{2+}-dependent gating underlying this diversity arises from multiple mechanisms, including alternate splicing of *Kcnma1*, the gene encoding the pore-forming (α) subunit of the BK channel, phosphorylation of α subunits, and inclusion of β subunits in channel complexes. To address the interplay of these mechanisms in the regulation of BK currents, two native splice variants, BK_0 and BK_{SRKR}, were cloned from a tissue that exhibits dynamic daily expression of BK channel, the central circadian pacemaker in the suprachiasmatic nucleus (SCN) of mouse hypothalamus. The BK_0 and BK_{SRKR} variants differed by the inclusion of a four–amino acid alternate exon at splice site 1 (SRKR), which showed increased expression during the day. The functional properties of the variants were investigated in HEK293 cells using standard voltage-clamp protocols. Compared with BK_0, BK_{SRKR} currents had a significantly right-shifted conductance–voltage (G-V) relationship across a range of Ca^{2+} concentrations, slower activation, and faster deactivation. These effects were dependent on the phosphorylation state of S642, a serine residue within the constitutive exon immediately preceding the SRKR insert. Coexpression of the neuronal β4 subunit slowed gating kinetics and shifted the G-V relationship in a Ca^{2+}-dependent manner, enhancing the functional differences between the variants. Next, using native action potential (AP) command waveforms recorded from SCN to elicit BK currents, we found that these splice variant differences persist under dynamic activation conditions in physiological ionic concentrations. AP-induced currents from BK_{SRKR} channels were significantly reduced compared with BK_0, an effect that was maintained with coexpression of the β4 subunit but abolished by the mutation of S642. These results demonstrate a novel mechanism for reducing BK current activation under reconstituted physiological conditions, and further suggest that S642 is selectively phosphorylated in the presence of SRKR.

The Journal of General Physiology

INTRODUCTION

The BK large-conductance calcium- and voltage-activated potassium channel ($K_{Ca}1.1$, MaxiK) is gated by both membrane depolarization and intracellular Ca^{2+} (Butler et al., 1993). BK channels are tetramers of four pore-forming α subunits (Shen et al., 1994), encoded by the *Kcnma1* (*Slo1*) gene (Butler et al., 1993; Meredith et al., 2004). BK α subunits are comprised of seven transmembrane domains (S0–S6) that form the channel pore and are responsible for voltage sensing and a cytoplasmic C-terminal domain that binds Ca^{2+} (Yuan et al., 2012). BK channels are expressed in a wide variety of excitable and nonexcitable cells (Tseng-Crank et al., 1994) where they have heterogeneous physiological functions. In neurons, BK channels contribute to the fast afterhyperpolarization of the action potential (AP) (Storm, 1987), AP duration and frequency (Storm, 1987; Montgomery et al., 2013), and neurotransmitter release (Robitaille and Charlton, 1992; Hu et al., 2001). In smooth muscle, BK currents limit contraction and promote relaxation (Brayden and Nelson, 1992; Brenner et al., 2000b). In nonexcitable cells, BK channels regulate K^+ homeostasis (Rieg et al., 2007) and hormone secretion (Petersen and Maruyama, 1984). Based on this wide array of cellular mechanisms, the BK channel has been implicated in the physiology of hearing (Fuchs and Evans, 1990; Pyott et al., 2007), circadian rhythmicity (Meredith et al., 2006), cardiovascular function (Sausbier et al., 2005), urination (Meredith et al., 2004), and locomotor function (Sausbier et al., 2004; Imlach et al., 2010).

Unlike many other K^+ channels, the BK channel tetramer is encoded by a single gene. Given this, physiological diversity of BK currents is achieved through several mechanisms including formation of macromolecular complexes with auxiliary subunits (Orio et al., 2002; Yan and Aldrich, 2012), posttranslational modification of α subunits (Tian et al., 2008; Yan et al., 2008), and alternative splicing (Shipston, 2001). Alternative splicing of *Kcnma1* transcripts has been proposed as a major mechanism driving the diversity of BK currents. Within the cytoplasmic C-terminal domain, four splice sites

C. Shelley and J.P. Whitt contributed equally to this paper.
Correspondence to Andrea L. Meredith: ameredith@som.umaryland.edu

Abbreviations used in this paper: AP, action potential; RCK, regulator of K^+ conductance; SCN, suprachiasmatic nucleus; STREX, stress axis–regulated exon.

The Rockefeller University Press $30.00
J. Gen. Physiol. Vol. 142 No. 6 585–598
www.jgp.org/cgi/doi/10.1085/jgp.201311072

have been identified. Site 1 is near the end of the first regulator of K^+ conductance (RCK) domain, containing either no insert or a four–amino acid alternate exon (SRKR) (Tseng-Crank et al., 1994). Site 2 is the stress axis–regulated exon (STREX) site, found within the linker between RCK1 and RCK2. This site can contain either no insert, a three–amino acid exon (IYF), a 61–amino acid exon (STREX1), the IYF and 61–amino acid exons (STREX2), or a 28–amino acid exon (Saito et al., 1997; Xie and McCobb, 1998; Chen et al., 2005). Site 3 is located near the high affinity Ca^{2+}-binding site (the "Ca^{2+} bowl") within RCK2 and can contain either no insert or a 27–amino acid alternate exon (Ha et al., 2000). Lastly, alternate exons at site 4 produce three distinct C termini ("VEDEC," "VYR," or "QEERL") (Saito et al., 1997).

Functionally, inclusion of alternate exons at each site produces effects on current properties that range in magnitude and mechanism, with the STREX site (site 2) being the most widely characterized. Inclusion of STREX1 or STREX2 enhances BK currents by speeding activation, slowing deactivation, and shifting the voltage dependence of activation more negative compared with insertless variants (Xie and McCobb, 1998; Chen et al., 2005). Depending on the Ca^{2+} concentration and the background splice variant sequence, inclusion of STREX can left-shift the $V_{1/2}$ up to 50 mV (Chen et al., 2005). Conversely, inclusion of the SRKR insert at site 1 was found to reduce BK currents by either right-shifting the $V_{1/2}$ (Tseng-Crank et al., 1994) or by reducing voltage sensitivity (Rosenblatt et al., 1997). Inclusion of the Ca^{2+}-bowl exon at site 3 does not have an appreciable effect on steady-state current properties; however, it does speed activation kinetics in a Ca^{2+}-dependent manner (Ha et al., 2000). Finally, the C-terminal exons so far appear to regulate trafficking and cell surface localization for the channel rather than significantly affecting current properties (Kim et al., 2008; Singh et al., 2013).

In addition to alternate splicing, posttranslational modifications, such as phosphorylation, have also been shown to underlie some of the physiological diversity in BK currents. The BK channel has ∼200 potentially phosphorylated serine and threonine residues. However, recent mass spectrometric analysis of rat brain BK protein detected only ∼30 endogenously phosphorylated residues (Yan et al., 2008). Some of these phosphorylated residues were found within alternative exons at sites 2, 3, and 4 (Yan et al., 2008), suggesting that the combinatorial effects of exon-specific phosphorylation could further contribute to BK current properties. Consistent with this, inclusion of the STREX insert (site 2) changes the phosphorylation dependence of activation. Phosphorylation of S869 in channels lacking the STREX insert increases channel activity, whereas phosphorylation of a serine within the STREX exon ($S4_{STREX}$) inhibits its channel activity (Tian et al., 2001). Although the phosphorylation dependence of STREX has been the most comprehensively studied, the functional impact of phosphorylation at other alternate exons has not been addressed.

In this study, we cloned and characterized two novel *Kcnma1* variants (BK_0 and BK_{SRKR}) from the mouse suprachiasmatic nucleus (SCN) of the hypothalamus, the brain's circadian clock. We chose to identify BK channel sequences from SCN because (a) BK currents undergo dynamic transcriptional regulation in this tissue, suggesting that multiple splice variants may be expressed (Panda et al., 2002; Pitts et al., 2006); (b) distinct AP waveforms have been characterized in SCN neurons that are hypothesized to exert differential influence on intrinsic currents (Colwell, 2011; Montgomery and Meredith, 2012); and (c) SCN expresses BK modulatory β subunits (Montgomery and Meredith, 2012). The BK_0 and BK_{SRKR} variants were identical except for the presence of a four–amino acid insert (SRKR) at splice site 1. To determine the functional effects of the SRKR insert, we expressed each variant with and without the β4 accessory subunit in HEK293 cells, eliciting currents in response to standard voltage jumps and representative "day" and "night" SCN AP waveform commands. Next, using a combination of phosphatase treatment and site-directed mutagenesis, we addressed the role of two serine residues, predicted to be phosphorylated in BK_{SRKR}, in generating the distinct current properties produced by the BK_0 and BK_{SRKR} variants. Lastly, using SCN AP commands and expression of β4 to reconstitute activation of BK currents under physiologically relevant conditions, we found that the differences in BK currents were expressed in response to the type of AP command, the splice variant expressed, the presence of the β4 subunit, and the phosphorylation status of S642.

MATERIALS AND METHODS

Cloning BK_0 and BK_{SRKR} variants from SCN

Total RNA was isolated from 10 pooled mouse SCNs harvested at zeitgeber time (ZT)6 (6 h after lights on), as described in Meredith et al. (2006). Total RNA was column purified (RNAeasy; QIAGEN), and cDNA was synthesized from 10 µg of total RNA (Superscript II; Invitrogen) using a gene-specific reverse primer (5′-GGTGACCATCATTCTCCTCAAAG-3′). PCR reactions amplifying the N-terminal (5′-ATGGCTGTTGATGGGTGTTCGGG-3′ and 5′-AGGCCCCCGAAGAAAGTCACCA-3′) or a single product containing splice sites 1–4 (5′-GAGTACAAGTCTGCCAACAG-3′ and 5′-CATTCAAATCAAGCCCATGAGTACCC-3′) were performed on 10 µl cDNA (Expand Taq; Roche). Products were gel purified, subcloned (pGEMTeasy; Promega), and sequenced to determine the presence of alternate exons at splice sites 1–4. Two PCR products were obtained with unique cDNA sequences, BK_0 and BK_{SRKR}.

A series of BK channel expression vectors containing the stepwise sequence additions and deletions of exons were introduced into mbr5 (Butler et al., 1993) in pcDNA3.1. In this study, mbr5 contained an N-terminal myc tag and EYFP (716 bp) inserted in the RCK2 domain at nucleotide position (nt) 2032 (GenBank

accession no. KF530038; provided by R. Brenner, The University of Texas at San Antonio, San Antonio, TX). Construct 2 (C2; GenBank accession no. KF530044; Fig. S1) contained an insertion of an N-terminal myc tag followed by 195 bp of additional *Kcnma1* N-terminal sequence encoding the "MANG" alternate start site. The inserted sequence was synthesized as a minigene (Integrated DNA Technologies), digested with KpnI/AgeI, and subcloned into mbr5/pcDNA3.1 at KpnI and BssHII sites.

For all subsequent constructs, splice site insertion or deletions were performed using site-directed PCR mutagenesis (QuikChange; Agilent Technologies) according to the manufacturer's protocol. For construct 3, three amino acids (IYF) were deleted from the STREX site by amplifying construct 2 with a primer containing a deletion of nts 2094–2102 (GenBank accession no. KF530036). For construct 4, 180 bp encoding the "VEDEC" C terminus was deleted by PCR from construct 3 (nts 4236–4415), and 21 bp encoding the "RKEMVYR" C terminus was introduced in a second PCR amplification (GenBank accession no. KF530042). BK_0 was generated by the addition of 78 bp encoding the 27–amino acid Ca^{2+}-bowl exon at nt 3564 in construct 4 (GenBank accession no. KF530040). BK_{SRKR} was generated by the addition of 12 bp encoding the SRKR exon at nt 1929 (GenBank accession no. KF530041).

Quantitative PCR

Total RNA was isolated from SCN tissue at 6 h after lights on (ZT6; "day") and 7 h after lights off (ZT19; "night") with the RNeasy mini kit (QIAGEN) as described previously (Montgomery and Meredith, 2012). Primers were as follows: SRKR, (F) 5′-GTTTTGTGAAGCTTAAGCTCCTGAT-3′ and (R) 5′-AGAGCCGAAGCCGAAAGC-3′; exon 16, (F) 5′-GTTTTGTGAAGCTTAAGCTCCTGAT-3′ and 5′-TCTCTCTGTTGGCAGACTTGTAC-3′. Real-time qPCR data were analyzed using the $2^{-\Delta\Delta Cq}$ method (Livak and Schmittgen, 2001). SRKR and exon 16 Cq values for day were normalized to the night values.

Predicted phosphorylation sites and mutagenesis of BK_0 and BK_{SRKR}

Sequence analysis for potential phosphorylation sites was performed online using NetPhos 2.0 (Blom et al., 1999). Predicted consensus phosphorylation sites received a score >0.9.

Mutation of predicted phosphorylation sites S642 and S644 was performed using site-directed PCR mutagenesis (QuikChange; Agilent Technologies). BK_0-S642D contained the mutation AGC to GAC at nts 1923–1925 (GenBank accession no. KF530040). BK_{SRKR}-S642A contained the mutation AGC to GCC at nts 1923–1935 (GenBank accession no. KF530041). BK_{SRKR}-S644A contained the mutation AGC to GCC at nts 1929–1931 (GenBank accession no. KF530041). All mutations were verified by sequencing.

HEK cell patch-clamp electrophysiology

HEK293T cells were transfected with BK expression constructs, with or without β4 in pcDNA3.1 (Wang et al., 2009). 1 µg DNA/35-mm dish was transfected for α subunits only, and 1 µg α plus 1.7 µg β4 was transfected for cotransfections, using Lipofectamine 2000 (Invitrogen). Cells were plated on glass coverslips 3–5 h later and recorded from 20 to 30 h after transfection. Patch-clamp recording was performed using the voltage-clamp mode in the inside-out patch configuration (Axopatch; Molecular Devices) using thin-walled borosilicate pipettes with resistances of 2–5 MΩ. Recordings were made at room temperature, and the data were acquired at 50 kHz and filtered at 10 kHz. Total $[Ca^{2+}]_i$ was calculated using Webmax C Standard software and the appropriate addition of $CaCl_2$ to achieve the indicated free Ca^{2+}. For 0 Ca^{2+} solutions, 5 mM EGTA was used, where free Ca^{2+} is expected to be <1 nM under these conditions (Bao et al., 2002). For 100-µM Ca^{2+} solutions, no EGTA was used. For inside-out patch recordings, the pipette (extracellular) solution was composed of (mM): 140 $KMeSO_3$, 2 KCl, 2 $MgCl_2$, and 20 HEPES, pH 7.3. The bath (intracellular) solution was composed of (mM): 140 $KMeSO_3$, 2 KCl, 20 HEPES, and 5 HEDTA for 1 and 10 µM of free Ca^{2+}. To elicit BK currents using voltage-jump protocols, patches were stepped from holding potentials of −100 to −150 to +350 mV (in 10-mV increments) for 20 ms (α alone) or 50 ms (α + β4), stepping back to −80 mV for 10 ms (α alone) or 20 ms (α + β4) to generate tail currents. Conductance (G) was calculated from tail currents, normalized to the highest conductance calculated for each patch, and plotted against membrane potential to generate G-V curves. Boltzmann functions were fitted to curves in Origin 8.5 (OriginLab) using the equation: $y = (A_1 - A_2)/(1 + e^{(x - x_0)/dx} + A_2$. Single-exponential functions were fitted to current traces in pCLAMP (Molecular Devices) to determine the time constants of activation, deactivation, and inactivation, using the equation $f(x) = A_i e(-t/\tau_i) + C$.

For dephosphorylation experiments, calf intestinal alkaline phosphatase (New England Biolabs, Inc.) was diluted to 10 U/ml in the intracellular bath solution. After recording baseline currents, phosphatase-containing solution (Alk P) was perfused into the bath, and posttreatment currents were recorded 5 min later.

Activation of BK currents by AP commands

AP command waveforms were originally recorded in whole-cell current-clamp mode from acute SCN slices during the day and night of the circadian cycle as described previously (Montgomery and Meredith, 2012). Day and night waveforms representative of the mean parameter values (see Results and Fig. 2 A) were used to elicit BK currents in whole-cell recording mode. The pipette (intracellular) solution was identical to the intracellular solution used in inside-out recordings, except with free Ca^{2+} adjusted to 50 µM. The bath (extracellular) solution consisted of (mM): 145 NaCl, 5 KCl, 2 $CaCl_2$, 1 $MgCl_2$, and 10 HEPES, with pH adjusted to 7.2 with NaOH. Cells were held at −100 mV. The applied voltage stimulation protocol consisted of a depolarizing prepulse to +160 mV for 20 ms, followed by either day or night physiological AP commands that included holding the cells at the appropriate physiological resting membrane potentials (−48.6 mV for day AP commands and −45.0 mV for night AP commands) for 50 ms before the actual AP commands (Fig. S3 A). Series resistance was compensated up to 60%.

For comparisons between splice variants, peak AP-elicited currents were normalized to the +160-mV prepulse (Fig. S3 B). For AP-induced BK currents, peak current was the difference between the baseline current at −100 mV and the maximum current observed in response to the AP command. Current half-width was the duration at 50% of the maximal current magnitude, measured between the current maximum and the afterhyperpolarization current. Charge transfer was calculated as the area of the normalized current from baseline (at resting membrane potential) to the maximum of the AP-induced current.

Statistics

Two-way ANOVAs with Bonferroni post-hoc analysis were used to determine statistical significance for differences between $V_{1/2}$ values and day versus night AP-induced current parameters for the BK variants, as indicated in the figure legends. One-way ANOVA was used for comparisons between wild-type and mutant AP-elicited currents (Fig. 4 H), and a *t* test was used to compare currents elicited by square voltage pulses in Fig. 4 G. Factorial ANOVAs with Bonferroni post-hoc analyses were used to determine statistical significance for τ_{act} and τ_{deact} between constructs elicited at different Ca^{2+} across a range of voltages. Statistical significance was achieved if $P \leq 0.05$. Mean values in figures are given as ±SEM.

Online supplemental material

Fig. S1 demonstrates that the addition of the alternate N terminus, deletion of residues IYF at site 2, and the addition of the alternate C terminus (RKEMVYR) have little effect on BK current properties. Fig. S2 demonstrates the functional differences produced by the addition of the Ca^{2+}-bowl exon at site 3 (BK_0) and the addition of SRKR at site 1 (BK_{SRKR}). Fig. S3 shows the prepulse voltage step used to normalize the AP-induced BK currents in relation to the AP voltage command and the BK currents elicited by each command to scale. Fig. S4 compares the amino acid sequences and secondary structures in the SRKR region from the two isoforms of the BK channel that have been crystallized to date. Table S1 contains the $V_{1/2}$ values of all the constructs used in this study. The online supplemental material is available at http://www.jgp.org/cgi/content/full/jgp.201311072/DC1.

RESULTS

Identification of two novel BK channel splice variants

To investigate BK current properties produced by native BK channels, we amplified full-length *Kcnma1* cDNAs from SCN, a tissue that exhibits dynamic expression of *Kcnma1* transcripts (Panda et al., 2002; Pitts et al., 2006). Two novel variants were identified (BK_0 and BK_{SRKR}; Fig. 1 A), containing an alternate exon combination that differed at four splice sites from previously identified BK variants. Both variants contained an alternate translation start encoded by additional sequence in the extracellular N terminus of the channel ("MANG"; Fig. 1 A). In addition, both variants lacked any insert at the STREX site (site 2), contained the 27–amino acid Ca^{2+}-bowl insert (site 3), and contained the same alternative C terminus, RKEMVYR (site 4). However, the variants differed from each other at splice site 1, located within RCK1, where BK_{SRKR} contains a four–amino acid insert, SRKR, that is absent in BK_0. Stepwise addition of each alternate sequence into a BK channel lacking inserts at splice sites 1 and 3, and replacements of exons at sites 2 and 4, revealed that the addition of the SRKR insert had the greatest impact on BK current properties (Figs. S1 and S2).

To determine whether the expression of BK transcripts containing the SRKR exon differed from the previously characterized nighttime-phased expression pattern of *Kcnma1* in SCN (Meredith et al., 2006; Montgomery and Meredith, 2012), exon 16 (the constitutive exon immediately preceding SRKR) and SRKR levels were determined by quantitative RT-PCR from day and night SCNs (Fig. 1 B). The abundance of transcripts containing exon 16 was greater at night compared with day (Fig. 1 B), similar to other constitutive *Kcnma1* exons (Panda et al., 2002; Pitts et al., 2006; not depicted). In contrast, the abundance of transcripts containing SRKR was higher during the day (Fig. 1 B), suggesting that SRKR-containing transcripts form a distinct type of BK channel that is regulated differentially with respect to circadian phase.

SRKR alters kinetic and steady-state BK current properties

Given the difference in abundance of SRKR-containing transcripts in day and night SCN tissue from the normal *Kcnma1* expression pattern, we looked at the functional impact of this exon on BK currents. BK_0 and BK_{SRKR} were expressed in HEK293 cells, and macroscopic BK currents were recorded from inside-out patches in symmetrical K^+ at 0, 1, 10, and 100 µM of intracellular Ca^{2+}. Expression of both variants produced BK currents that activated with increasing depolarization and Ca^{2+} (Fig. 2 A). Differences in current properties were apparent at 0, 1, and 100 µM, where the BK_{SRKR} G-V relationship was right-shifted compared with BK_0, but not at 10 µM Ca^{2+} (Fig. 2 B). At 100 µM Ca^{2+}, a condition where all of the high affinity Ca^{2+}-binding sites are expected to be occupied, BK_{SRKR} currents were harder to activate relative to BK_0, with the $V_{1/2}$ right-shifted by 19 mV compared with BK_0 (Fig. 2 C). This effect was also seen at 1 µM Ca^{2+} (+35-mV right-shift), as well as in the absence of Ca^{2+}

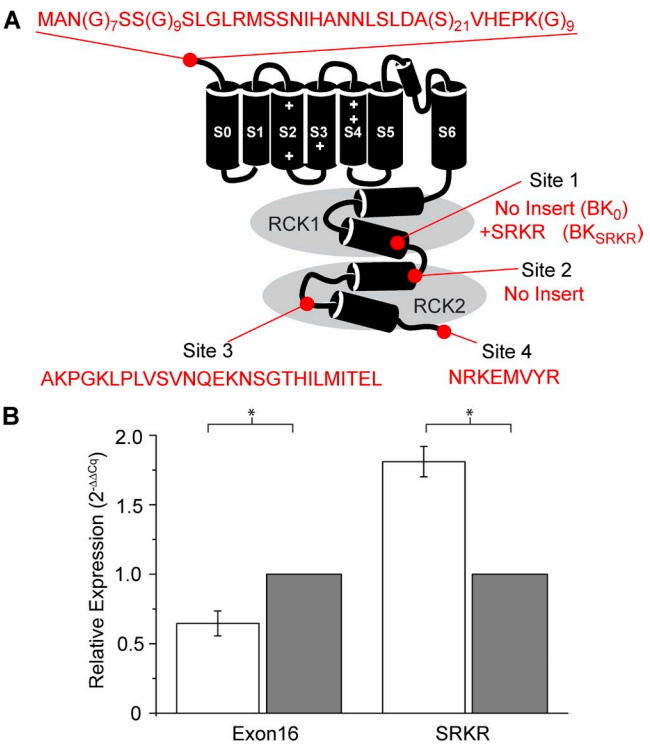

Figure 1. Native BK channel splice variants expressed in the SCN. (A) Schematic of the BK channel. Both BK_0 and BK_{SRKR} contain an extended N-terminal region ("MANG"), no insert at site 2 (STREX), a 27–amino acid insert at site 3 ("Ca^{2+} bowl"), and the "VYR" C terminus. In addition, BK_{SRKR} includes the SRKR insert at splice site 1. (B) The day (open bars) and night (closed bars) expression of the alternate exon SRKR differs from the constitutive exon 16. Relative expression levels were determined by quantitative RT-PCR and normalized to the nighttime value for each reaction. Expression of transcripts containing exon 16 was significantly higher at night ($n = 3$; $P = 0.0023$; *t* test), whereas expression of SRKR-containing transcripts was higher during the day ($n = 3$; $P = 0.015$; *t* test).

(+49-mV right-shift). There was no change in the slope factor (voltage sensitivity) between BK_0 and BK_{SRKR} G-Vs at each Ca^{2+} concentration. These data show that inclusion of the SRKR exon shifts the voltage dependence of activation to more positive values across a range of membrane potentials. Surprisingly, there was no significant difference in the $V_{1/2}$ values of BK_{SRKR} and BK_0 G-Vs at the intermediate Ca^{2+} concentration of 10 µM (Fig. 2, B and C).

There were also differences in the kinetics of activation and deactivation between BK_0 and BK_{SRKR} currents. At 0, 1, and 100 µM Ca^{2+}, the time constants of activation (τ_{act}) for BK_{SRKR} currents were increased compared with BK_0 (Fig. 2 D). This slowing of activation was particularly pronounced at 100 µM Ca^{2+} at more negative voltages (Fig. 2 E). As with the steady-state G-V data, there was no difference in BK_0 and BK_{SRKR} current activation time constants in the intermediate Ca^{2+} concentration of 10 µM. BK_{SRKR} currents showed decreased τ_{deact} at 100, 1, and 0 µM Ca^{2+} with no significant effect at 10-µM Ca^{2+} concentrations (Fig. 2 F). Overall, at saturating (100 µM) Ca^{2+}, the right-shifted $V_{1/2}$, increased activation time constants, and decreased deactivation time constants would be expected to reduce native BK_{SRKR} currents compared with BK_0. The same effect is expected at low Ca^{2+} (0 and 1 µM), where BK_{SRKR} currents were similarly right-shifted and slower to activate compared with BK_0, but absent at intermediate Ca^{2+} (10 µM), where no significant differences in current properties were observed.

SRKR is required for phosphoregulation of serine 642

BK_0 and BK_{SRKR} splice variants differ by only four amino acids, yet they have substantial differences in both steady-state and kinetic properties. Given the presence of a serine within the SRKR insert, we hypothesized that phosphorylation of this residue (S644; Fig. S4) could contribute to the difference in BK_0 and BK_{SRKR} current properties. Analysis of SRKR and the surrounding sequence in BK_{SRKR} with a phosphorylation prediction

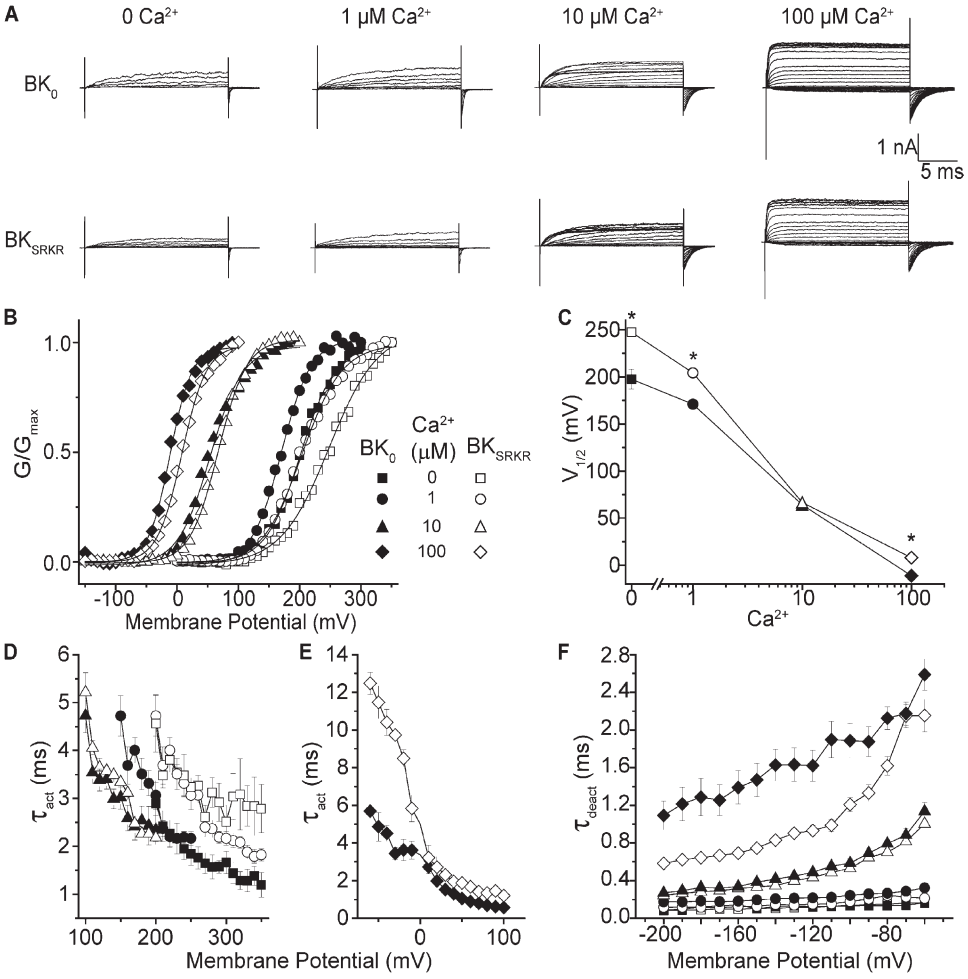

Figure 2. Voltage-clamp recordings and analysis of BK_0 and BK_{SRKR} currents from variants expressed in HEK293 cells. (A) Current traces from BK_0 and BK_{SRKR} patches elicited from voltage jumps at the indicated intracellular Ca^{2+}. (B) Normalized G-V relationship for BK_0 and BK_{SRKR} at different Ca^{2+}. There was no significant differences in the slopes of the G-V curves between BK_0 and BK_{SRKR} at each Ca^{2+} concentration ($P = 0.07$; two-way ANOVA). (C) Plot of $V_{1/2}$ versus Ca^{2+} exemplifying the difference in voltage dependence of activation between BK_0 and BK_{SRKR}. $V_{1/2}$ values were significantly different between BK_0 and BK_{SRKR} at 0 Ca^{2+} (198 vs. 247 mV; $P < 0.01$; $n = 8$; two-way ANOVA), 1 µM Ca^{2+} (169 vs. 204 mV; $P < 0.01$; $n = 8$; two-way ANOVA), and 100 µM Ca^{2+} (−11 vs. 8 mV; $P < 0.01$; $n = 8$; two-way ANOVA). No significant difference in $V_{1/2}$ was detected at 10 µM Ca^{2+} (64 vs. 67 mV; $P = 0.1$; $n = 8$; two-way ANOVA). (D and E) Plot of τ_{act} versus voltage for BK_0 and BK_{SRKR} at 0, 1, and 10 µM Ca^{2+} (D) and 100 µM Ca^{2+} (E). Activation of BK_0 was significantly faster than BK_{SRKR} at 0, 1, and 100 µM ($P < 0.01$; factorial ANOVA), but not at 10 µM Ca^{2+}, where no differences in kinetics were observed. All symbols as in B. (F) Plot of τ_{deact} versus voltage for BK_0 and BK_{SRKR} at 0, 1, 10, and 100 µM Ca^{2+}. Deactivation of BK_0 was significantly slower than BK_{SRKR} with 0, 1, and 100 µM Ca^{2+}, but not with 10 µM Ca^{2+} ($P < 0.01$; factorial ANOVA). All symbols as in B. In cases where error bars are not present, the bars were smaller than the data symbol.

algorithm (Blom et al., 1999) indicated a high probability for S644 phosphorylation (NetPhos score of 0.991). S642, a constitutive residue preceding the SRKR insert (Fig. S4), also had a high probability score for phosphorylation (NetPhos score of 0.994). In contrast, in the BK_0 sequence, which lacked SRKR, the constitutive S642 had a significantly lower probability of phosphorylation (0.557). These results predicted that phosphorylation of S642 and/or S644 may occur in BK_{SRKR}, but not in BK_0, channels.

First, to determine if net phosphorylation of BK_{SRKR} could explain the differences in current properties compared with BK_0, we applied alkaline phosphatase to the intracellular side of macropatches. At 100 μM Ca^{2+}, the BK_{SRKR} G-V curve was right-shifted compared with BK_0. In the presence of phosphatase, the BK_{SRKR} $V_{1/2}$ was left-shifted by 14 mV, making it similar to that of BK_0 and significantly different from that of BK_{SRKR} (Fig. 3, A and B). This result suggested that dephosphorylation increased BK_{SRKR} channel activity to match that of BK_0. In contrast, the application of phosphatase had no effect on BK_0 currents (Fig. 3, A and B), confirming that the SRKR insert is required to render the currents susceptible to phosphatase. These experimental results are consistent with the high phosphorylation probability

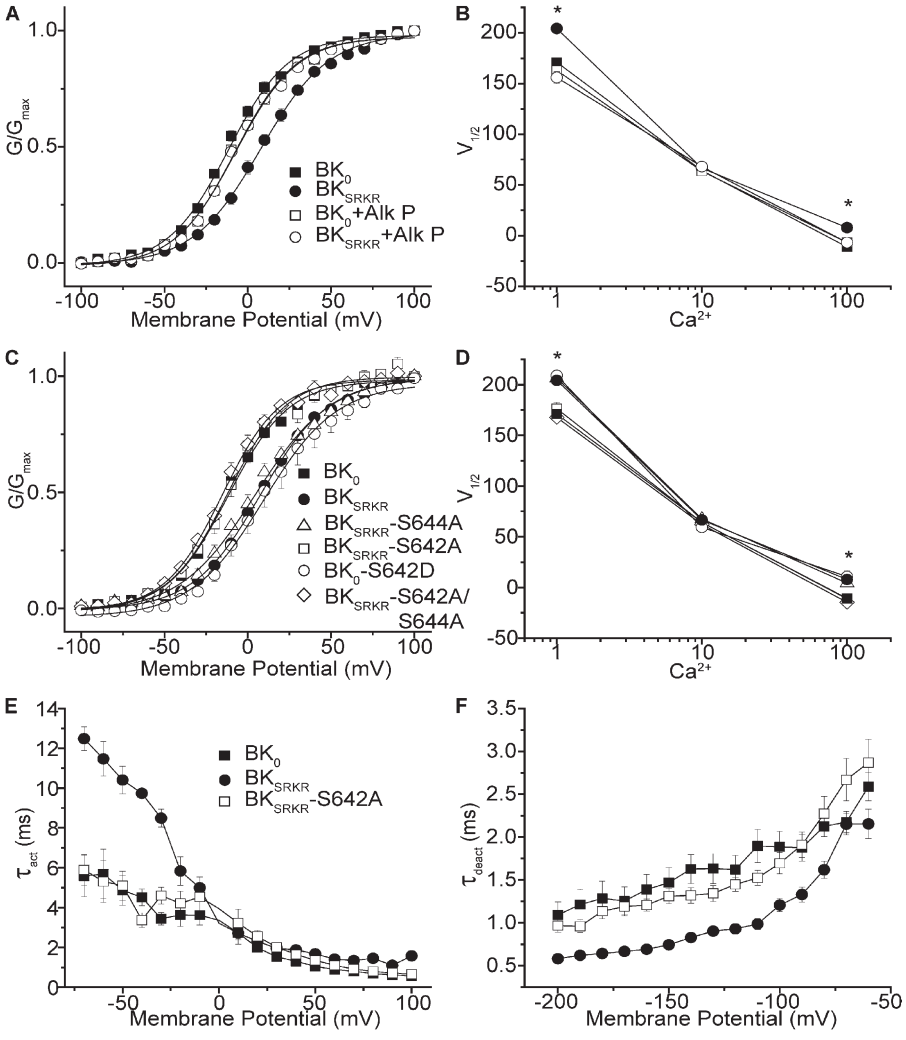

Figure 3. BK_0 and BK_{SRKR} current properties in patches treated with phosphatase or from phospho-site mutants. (A) G-V relationship of BK_0 and BK_{SRKR} at 100 μM Ca^{2+} before and after the application of calf intestinal alkaline phosphatase (Alk P). Alk P caused a leftward shift of the BK_{SRKR} G-V, but not of BK_0 G-V. (B) Plot of $V_{1/2}$ versus Ca^{2+}, illustrating that dephosphorylation of BK_{SRKR} produces a BK_0-like phenotype in the voltage dependence of activation. After treatment with phosphatase, the $V_{1/2}$ was significantly left-shifted with BK_{SRKR} at 1 μM Ca^{2+} (204–155 mV; P = 0.01; n = 8; two-way ANOVA) and at 100 μM Ca^{2+} (8 to −6 mV; P = 0.03; n = 8; two-way ANOVA), but not with BK_0 at either 1 μM Ca^{2+} (169–156 mV; P = 0.25; n = 8; two-way ANOVA) or 100 μM Ca^{2+} (−11 vs. −7 mV; P = 0.53; n = 8; two-way ANOVA), making the phosphatase-treated BK_{SRKR} not significantly different from BK_0 (P = 0.7; n = 8). Symbols are as in A. (C) G-V relationship at 100 μM Ca^{2+} of specific phospho-mutants used to determine the site of differential phospho-regulation of BK_{SRKR}. Phospho-mutant BK_{SRKR} S644A, the S in SRKR, had no effect on G-V relationship, whereas phosphomimetic BK_{SRKR} S642D, found within a constitutive portion of the channel, was found to be necessary and sufficient to induce that change in current properties. (D) Plot of $V_{1/2}$ versus Ca^{2+} for BK constructs shown in C. At 1 and 100 μM Ca^{2+}, the $V_{1/2}$ values cluster into two groups, with those of BK_{SRKR}, BK_{SRKR}-S644A, and BK_0-S642D further right-shifted than those of BK_0, BK_{SRKR}-S642A, and BK_{SRKR}-S642A/S644A. Symbols are as in C. At 1 μM Ca^{2+}, there were no significant differences in the $V_{1/2}$ values between BK_{SRKR} and BK_{SRKR}-S644A (204 and 206 mV; P = 0.29; n = 8–12; two-way ANOVA), between BK_{SRKR}-S642A and BK_0 (166 and 169 mV; P = 0.29; n = 8–10; two-way ANOVA), between BK_0-S642D and BK_{SRKR} (209 vs. 204 mV; P = 0.76; n = 8; two-way ANOVA), or between BK_{SRKR}-S642A/S644A and BK_0 (167 vs. 169 mV; P = 0.25; n = 8–15; two-way ANOVA). At 100 μM Ca^{2+}, there were no significant differences in the $V_{1/2}$ values between BK_{SRKR} and BK_{SRKR}-S644A (6 and 8 mV; P = 0.3; n = 8; two-way ANOVA), between BK_{SRKR}-S642A and BK_0 ($V_{1/2}$ values both −11 mV; P = 0.6; n = 8; two-way ANOVA), between BK_0-S642D and BK_{SRKR} (11 vs. 8 mV; P = 0.4; n = 8; two-way ANOVA), or between BK_{SRKR}-S642A/S644A and BK_0 (−15 vs. −11 mV; P = 0.6; n = 8; two-way ANOVA). (E and F) Plots of τ_{act} (E) and τ_{deact} (F) versus voltage for BK_0, BK_{SRKR}, and BK_{SRKR}-S642A at 100 μM Ca^{2+}. Activation kinetics of BK_{SRKR}-S642A were not significantly different to those of BK_0 (P = 0.34; n = 8) but were significantly slowed compared with BK_{SRKR} (P = 0.02; n = 8–9; factorial ANOVA). Similarly, deactivation kinetics of BK_{SRKR}-S642A were not significantly different to those of BK_0 (P = 0.49; n = 8; factorial ANOVA) but were significantly slowed compared with BK_{SRKR} (P < 0.01; n = 8–9; factorial ANOVA).

score for the BK_{SRKR} variant and low probability score for the BK_0 variant.

Next, to determine if a serine residue was required within the SRKR insert, we mutated S644 to an alanine. We hypothesized that currents produced from BK_{SRKR}-S644A mutants would resemble both BK_0 and the phosphatase-treated BK_{SRKR} currents. Surprisingly, BK_{SRKR}-S644A showed no difference in the G-V relationship compared with wild-type BK_{SRKR} (Fig. 3, C and D). Furthermore, phosphatase treatment of BK_{SRKR}-S644A still left-shifted the G-V curve to match that of BK_0 (not depicted). Collectively, these results suggested that dephosphorylation is occurring at a residue other than S644 to produce the observed functional effects.

Next, we focused on S642, a constitutive serine present in both BK_0 and BK_{SRKR} variants. We hypothesized that in the absence of SRKR, S642 would be resistant to phosphorylation. Conversely, the presence of the SRKR insert may render S642 permissive to phosphorylation, leading to the observed right-shifted G-V curve for BK_{SRKR} currents. To test this prediction, S642 was mutated to alanine. Confirming the role of this serine in the functional current differences, the G-V curve of BK_{SRKR}-S642A matched that of BK_0 (Fig. 3, C and D). Furthermore, the introduction of the converse phosphomimetic mutation into BK_0, BK_0-S642D, produced a right-shifted G-V curve that matched that of BK_{SRKR} (Fig. 3, C and D). These results identify S642 as the critical residue underlying the differences in BK_{SRKR} current properties compared with BK_0 and suggest that phosphorylation of S642 decreases channel activity.

Mutating both serine residues to alanine in BK_{SRKR} (BK_{SRKR}-S642A/S644A) resulted in G-V curves that matched those of BK_0 (Fig. 3, C and D), and no further left-shift of the G-V was produced by phosphatase treatment of this mutant (not depicted). These data confirm that no additional phosphorylation sites (sensitive to this phosphatase) were involved in the G-V differences between BK_0 and BK_{SRKR}. Quantitatively similar results were obtained when the phosphatase and mutagenesis experiments were repeated at 1 µM Ca^{2+} (Fig. 3 D). However, at 10 µM Ca^{2+}, in which no functional differences in the currents produced by BK_0 and BK_{SRKR} were observed (Fig. 2), neither phosphatase treatment nor mutagenesis altered the G-V curves (Fig. 3, B and D).

In addition to steady-state current properties, mutation of S642 also impacted current kinetics. We found that the time constants of both activation and deactivation of BK_{SRKR}-S642A were similar to those of BK_0 (Fig. 3, E and F). Thus, both the steady-state and kinetics properties of BK_{SRKR} lacking the S642 phosphorylation site resemble those of BK_0.

SRKR reduces BK currents elicited by AP commands

Much of the previously published work on BK current properties produced by specific variants has examined currents in response to standard square voltage-pulse protocols. Few studies have addressed the properties of BK currents elicited by a more physiologically relevant stimulus, such as an AP. Therefore, we recorded BK currents elicited from two distinct types of AP waveforms (day and night), based on recordings from SCN neurons where BK_0 and BK_{SRKR} are endogenously expressed. These experiments examined whether splice variant–based differences in BK currents were still apparent in response to physiologically relevant activation. We also examined currents elicited under these conditions coexpressed with β4, the major neuronal auxiliary subunit, which is known to be expressed within the SCN (Montgomery and Meredith, 2012).

The representative day and night AP waveforms used as a voltage command for BK current activation were obtained from whole-cell recordings of spontaneously firing neurons during the peak (day) and trough (night) of neural activity (Montgomery and Meredith, 2012). Day and night AP waveforms differed significantly in several parameters (Montgomery and Meredith, 2012), including peak depolarization (14.9 mV for day compared with −2.2 mV for night), half-width (2.1 vs. 3.0 ms, respectively), and baseline membrane potential (−48.6 vs. −45.0 mV, respectively). These distinct AP properties were expected to exert a differential drive on BK activation, conditions that might alter the expression of the differences observed under square voltage-jump conditions between BK_0 and BK_{SRKR} currents.

Day and night AP command waveforms (Fig. 4 A) were used to elicit currents in physiological ion concentrations (low internal K^+ and high external Na^+). Fig. 4 B shows AP-elicited currents from BK_0 and BK_{SRKR}, elicited from day or night AP command waveforms at 50 µM Ca^{2+}, mimicking the high local Ca^{2+} concentration experienced by BK channels in vivo coupled with voltage-gated Ca^{2+} channels (Fakler and Adelman, 2008). In this configuration, the time course of the BK currents generally followed the depolarizing phase of the AP command waveforms, mirroring the differences seen between the day and night AP properties. To directly compare BK_0 and BK_{SRKR} properties across cells expressing different levels of each channel variant, the AP-elicited currents were normalized to a maximally activating depolarizing prepulse step (Fig. S3). The mean AP-induced peak currents from both variants were very low, ranging from 2 to 8% of maximal current, depending on the variant and AP command waveform. Both BK_0 and BK_{SRKR} currents elicited by day AP commands had significantly increased peak current amplitudes and decreased half-widths compared with currents elicited by night AP commands (Fig. 4, D and F). There was no significant difference in charge transfer elicited by day and night AP commands (Fig. 4, E and F). These data show that the day and night AP command waveforms produced differing drives on BK current activation under standardized conditions.

Next, we compared the properties of BK_0 and BK_{SRKR} currents to each other, using either day or night AP commands (Fig. 4 C). BK_0 and BK_{SRKR} currents elicited by the same stimulus, either the day or night AP command waveform, showed different properties (Fig. 4 C). BK_{SRKR} had significantly decreased peak currents (Fig. 4 D), decreased charge transfer (Fig. 4 E), and increased current half-width (Fig. 4 F) compared with BK_0. These results are consistent with our findings using standard voltage jumps (Fig. 2 B).The reduced BK_{SRKR} currents compared with BK_0 elicited by AP commands could be caused by differences in the steady-state properties of the channels, kinetic properties, or a combination of both. To determine whether reduced steady-state activation could explain the differences between BK_0 and BK_{SRKR} AP-induced currents, we used a square pulse of 40 ms to depolarize cells to +14.9 mV, the peak voltage achieved using the day AP command. We found no significant difference between BK_0 and BK_{SRKR} currents under these conditions (Fig. 4 G), indicating that differences in steady-state parameters are not responsible for the distinct AP-induced BK_0 and BK_{SRKR} current properties. This suggests that kinetic differences account for the major differences in currents produced by the two variants elicited by AP commands.

Because S642 is critical for expression of the differences between BK_0 and BK_{SRKR} currents under standard voltage-jump protocols, we next sought to determine whether removal of the phosphorylation site S642 in the BK_{SRKR} variant would render channels "BK_0-like" in their responses to AP command waveforms. BK_{SRKR}-S642A currents elicited by the day AP command were

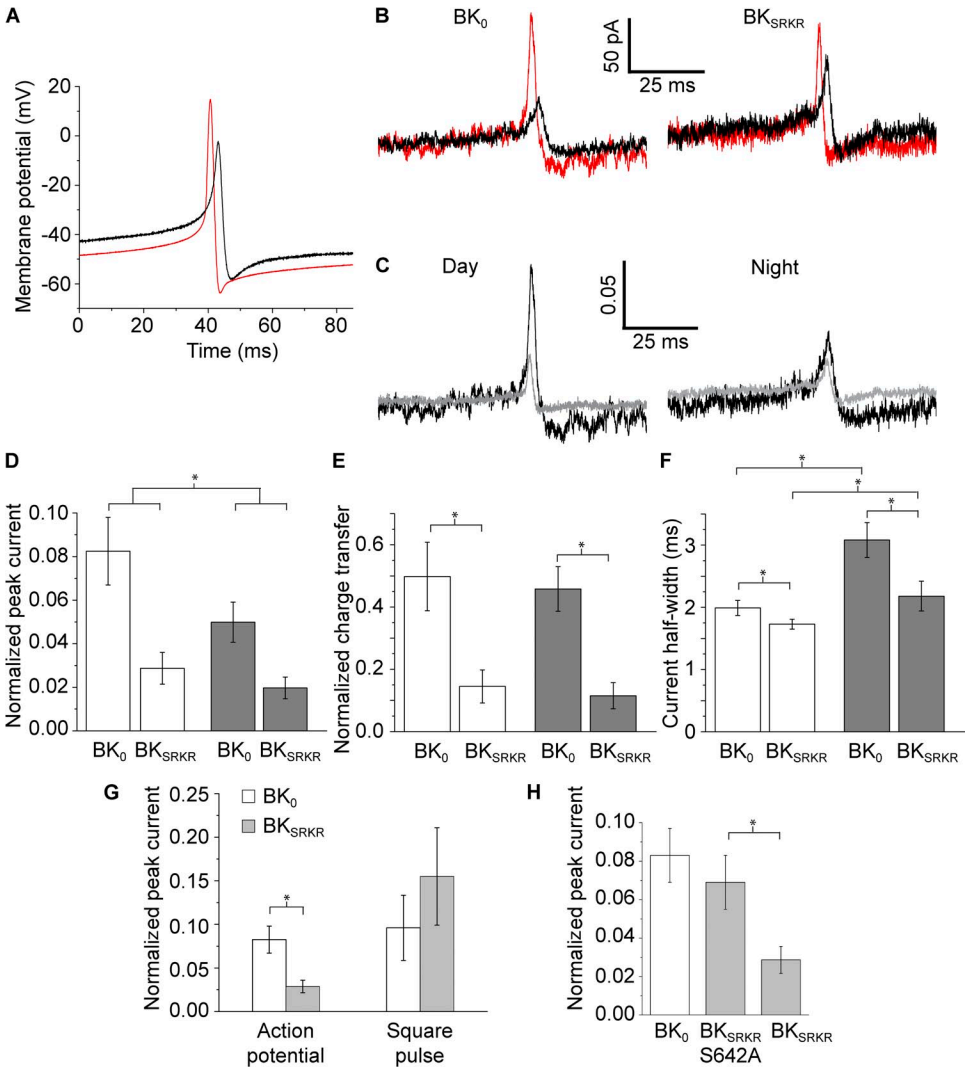

Figure 4. BK_{SRKR} and BK_0 currents elicited from AP commands in HEK293 cells. (A) Day (red) and night (black) AP commands, recorded from SCN neurons. (B) Currents elicited from BK_0 and BK_{SRKR} in physiological K^+ at 50 µM Ca^{2+} in response to either day (red) or night (black) AP commands in A. (C) BK_0 (black) and BK_{SRKR} (gray) currents elicited from day (left) and night (right) AP commands, normalized to the peak steady-state current in response to a +160-mV step. (D–F) Mean normalized peak current (D), charge transfer (E), and half-width (F) values for BK_0 and BK_{SRKR} currents elicited by day (open bars) and night (closed bars) AP commands. For both splice variants, currents induced by day versus night AP commands had significantly greater peak current amplitude ($P = 0.04$; two-way ANOVA) and significantly reduced half-width ($P < 0.01$; two-way ANOVA) compared with currents elicited from night APs. There was no significant difference in charge transfer between day and night. Comparing the values between splice variants, BK_{SRKR} currents were reduced compared with BK_0 currents using both day and night AP commands, as shown by the increased peak current, charge transfer, and half-width ($P < 0.01$ for all BK_0 and BK_{SRKR} comparisons; $n = 9$–11 for all conditions; two-way ANOVA). (G) Normalized peak currents for BK_0 and BK_{SRKR} elicited from day AP commands were significantly different, whereas those elicited from a square voltage pulse of the same magnitude of the day AP were not significantly different ($P = 0.4$; $n = 3$–11; t test). (H) Normalized peak currents in response to day AP commands from BK_{SRKR}-S642A were not significantly different from BK_0 ($P > 0.5$; one-way ANOVA) but were significantly different from BK_{SRKR} ($P = 0.05$; $n = 9$–11; one-way ANOVA).

significantly larger than wild-type BK_{SRKR} currents, and were similar to BK_0 peak currents (Fig. 4 H). This result suggests that phosphorylation of S642 in BK_{SRKR} channels would be expected to alter BK currents activated during the AP, opening the possibility that the SRKR splice site could play a role in influencing neural activity.

β4 enhances the functional differences between BK_0 and BK_{SRKR}

In vivo, BK current properties are modified by association with accessory β subunits. In the SCN (Montgomery and Meredith, 2012) and the brain as a whole, β4 is the predominant BK modulatory subunit (Behrens et al., 2000; Brenner et al., 2000a). Coexpression of β4 with the mbr5 BK channel has been shown to exert complex effects, decreasing Ca^{2+} sensitivity at low Ca^{2+} and increasing Ca^{2+} sensitivity at high Ca^{2+}, with little effect at 10 µM Ca^{2+} (Behrens et al., 2000; Brenner et al., 2000a; Lippiat et al., 2003; Wang et al., 2006). β4 also influences channel kinetics, slowing rates of both activation and deactivation (Behrens at al., 2000; Brenner et al., 2000a). To examine the influence of β4 on each splice variant, and to determine whether β4 affects the functional differences observed between the splice variants, we coexpressed β4 with either BK_0 or BK_{SRKR}. First, currents were recorded from inside-out patches in symmetrical K^+ solutions with standard square voltage jumps (Fig. 5 A), and G-V relationships and activation and deactivation kinetics were examined (Fig. 5, B–G). Similar to the previously reported effects on other BK channel variants, coexpression of β4 slowed activation of both BK_0 and BK_{SRKR} at both 10 and 100 µM Ca^{2+} (Fig. 5, A and B). At 10 µM Ca^{2+}, β4 slowed the activation time constants of BK_0 and BK_{SRKR} to a comparable degree. Thus, the activation time constants at 10 µM Ca^{2+} were similar between the variants with and without β4 (Figs. 2 D and 5 B).

In contrast, at 100 µM Ca^{2+}, although β4 slowed the activation of both BK_0 and BK_{SRKR}, the relative differences in activation kinetics between the variants in the

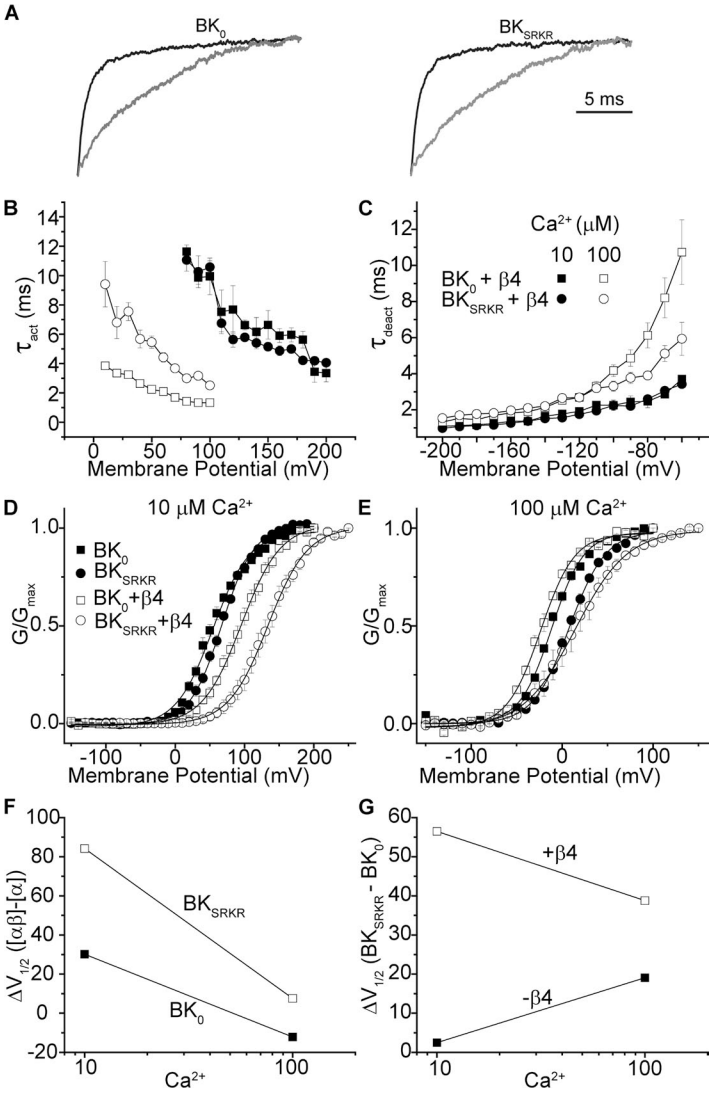

Figure 5. BK_0 and BK_{SRKR} currents from variants coexpressed with β4. (A) BK_0 and BK_{SRKR} currents were elicited with voltage steps from −100 to 200 mV with 10 µM Ca^{2+}. Current traces were normalized to I_{max} elicited from either the α subunit alone (black) or coexpressed with β4 (gray traces). (B and C) Plot of τ_{act} (B) or τ_{deact} (C) versus voltage for BK_0 and BK_{SRKR} coexpressed with β4 at 10 and 100 µM Ca^{2+}. Symbols are as in C. Although no difference is found in kinetics between the two variants at 10 µM Ca^{2+}, BK_{SRKR} was significantly ($P < 0.01$; factorial ANOVA) slower to activate and faster to deactivate ($P < 0.01$) when coexpressed with β4 at 100 µM Ca^{2+}. (D and E) G-V relationships of BK_0 and BK_{SRKR} coexpressed with β4 at 10 µM Ca^{2+} (D) and 100 µM Ca^{2+} (E). $V_{1/2}$ values were significantly different between BK_0 and BK_{SRKR} at both 10 µM Ca^{2+} (151 vs. 94 mV; $P < 0.01$; $n = 8$; two-way ANOVA) and at 100 µM Ca^{2+} (15 vs. −23 mV; $P < 0.01$; $n = 8$; two-way ANOVA). (F) Plot of $\Delta V_{1/2}$ versus Ca^{2+} for each splice variant caused by β4 expression ($V_{1/2}[\alpha\beta] - V_{1/2}[\alpha]$). Increasing Ca^{2+} reduces the $V_{1/2}$ shift caused by β4 for both variants, albeit to differing extents. (G) Plot of $\Delta V_{1/2}$ versus Ca^{2+} between variants ($V_{1/2}[BK_{SRKR}] - V_{1/2}[BK_0]$). The addition of β4 increases the difference in $V_{1/2}$ between splice variants.

presence of β4 were increased at positive voltages (Fig. 5 B) compared with activation kinetics in the absence of β4 (Fig. 2 E). The net effect was a larger divergence in activation time constants between the variants when β4 was coexpressed with 100 μM Ca^{2+}.

β4 also slowed deactivation of both splice variants at 100 μM Ca^{2+}, while still maintaining the faster deactivation of BK_{SRKR} compared with BK_0 at more depolarized potentials (Fig. 5 C). In the absence of β4, differences in BK_0 and BK_{SRKR} deactivation were most apparent at potentials hyperpolarized to approximately −100 mV (Fig. 2 B). However, in the presence of β4, increasing voltage caused a widening divergence of deactivation time constants between BK_0 and BK_{SRKR} (Fig. 5 C). At 10 μM Ca^{2+}, β4 also slowed deactivation of both variants approximately fourfold. As with activation time constants, the deactivation time constants of the two variants at 10 μM Ca^{2+} in the absence of β4 were similar (Fig. 2 F), and β4 coexpression did not introduce any further relative differences between BK_0 and BK_{SRKR}.

Although β4 coexpression did not affect the differences in kinetics of activation or deactivation between the variants at 10 μM Ca^{2+}, it did influence the G-V relationship. At 10 μM Ca^{2+}, the presence of β4 right-shifted the $V_{1/2}$ values for BK_0 and BK_{SRKR} by 30 and 84 mV, respectively (Fig. 5, D and F, and Table S1). Furthermore, although in the absence of β4 at 10 μM Ca^{2+} no difference was seen between the G-V curves of BK_0 and BK_{SRKR} (Fig. 2, B and E), coexpression with β4 now produced a 57-mV difference in $V_{1/2}$ values (Fig. 5 G).

In contrast to 10 μM Ca^{2+}, at 100 μM Ca^{2+}, β4 coexpression was found to have much reduced, but opposing, effects on the G-V curves. For BK_0, the addition of β4 left-shifted the $V_{1/2}$ by 12 mV; however, in the case of BK_{SRKR}, β4 caused a 7-mV right-shift (Fig. 5, E and F, and Table S1). Coexpression of β4 increased the differences in $V_{1/2}$ between the variants, although to a lesser extent than at 10 μM Ca^{2+} (Fig. 5 G). These results demonstrate that β4 coexpression acts to increase the functional differences between the steady-state properties of the splice variants at 10 and 100 μM Ca^{2+}.

We next examined the consequence of β4 coexpression on the splice variant responses to day and night SCN AP waveforms. Whole-cell currents were recorded with physiological solutions (low internal K^+ and high external Na^+) at 50 μM of internal Ca^{2+}. In response to night AP commands, β4 coexpression led to a significant twofold increase in BK_0 peak current compared with BK_0 alone (Fig. 6 B). This effect was consistent with the left-shifted G-V from BK_0/β4 currents at a similar high Ca^{2+} (Fig. 5 E). In contrast, BK_{SRKR} peak currents elicited by night AP commands were not significantly enhanced by coexpression of β4, agreeing with the modestly right-shifted G-V for BK_{SRKR}/β4. In addition, β4 had no significant effect on either BK_0 or BK_{SRKR} currents elicited by day AP commands (Fig. 6, A and B). These results show that β4 differentially affects the BK_0 and BK_{SRKR} splice variants under distinct stimulus conditions, an effect that is consistent with results obtained in symmetrical K^+ conditions (Fig. 5).

Because BK_{SRKR} peak currents were reduced compared with BK_0 in response to both day and night AP commands without β4, we compared the magnitude of the decrease in BK_{SRKR} peak current in the presence of β4 (Fig. 6). In response to the night AP command without β4, BK_{SRKR} currents were decreased by 2.5-fold compared with BK_0. In the presence of β4, this difference widened to threefold (Fig. 6 B). In contrast, the day AP command produced a significant 2.8-fold reduction in BK_{SRKR} current compared with BK_0 in the absence of β4, which was blunted to a 2.1-fold reduction by the addition of β4 (Fig. 6 A). Furthermore, in the presence of β4, BK_{SRKR} peak currents were no longer statistically different to BK_0 because of an increase in the variability with β4 coexpression. Collectively, these results suggest that β4 plays a greater role in modulating the differences between BK_0 and BK_{SRKR} currents in response to night AP commands than in response to day AP commands.

DISCUSSION

In this study, we identified two BK channel splice variants containing novel combinations of alternate exons

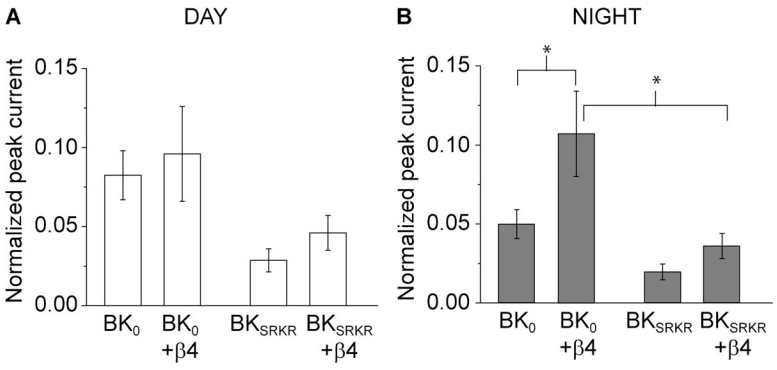

Figure 6. β4 effects on AP-induced currents. (A and B) Normalized peak currents for BK_0 and BK_{SRKR} elicited by day (A) and night (B) AP commands, expressed with and without β4. In the absence of β4, BK_{SRKR} currents were significantly reduced compared with BK_0 for both day and night AP commands ($P < 0.05$; data replotted from Fig. 4 to facilitate comparisons; two-way ANOVA). Coexpression of β4 had no significant effect on peak current from either splice variant elicited by day AP commands. In contrast, β4 significantly increased BK_0 peak currents ($P < 0.01$; two-way ANOVA), preserving the significant difference in BK_0 + β4 and BK_{SRKR} + β4 peak currents ($P < 0.01$; $n = 5–11$; two-way ANOVA). For clarity, significant differences are only marked for pairwise comparisons involving β4.

(BK_0 and BK_{SRKR}), which differed from each other by a four–amino acid insert (Fig. 1). We determined that the functional differences between BK_0 and BK_{SRKR} currents were caused by the SRKR exon (Fig. 2). Inclusion of the SRKR exon (BK_{SRKR}) resulted in a large reduction of BK channel activity, demonstrated by a rightward shift in G-V relationships, slower activation rates, and faster deactivation rates. These effects were abrogated by dephosphorylation only when SRKR was present and, conversely, could be reproduced in the absence of SRKR by a phosphomimetic mutation (S642D) (Fig. 3). Overall, the changes in current properties caused by SRKR were larger than those caused by the inclusion of other alternate exons at sites 2, 3, and 4 (Figs. S1 and S2, and Table S1). When BK_{SRKR} was examined in a reconstituted physiological system activated by neuronal AP commands in saturating Ca^{2+}, we found that even with the slower rate of depolarization and the much shorter duration of AP commands compared with voltage jumps, BK_{SRKR} still had reduced activity compared with BK_0. This inhibition was manifested as a reduction in peak current, charge transfer, and current half-width during the AP stimulus compared with BK_0 and was eliminated by mutation of S642 (Fig. 4). Collectively, the central finding of this study establishes the context-dependent phosphorylation of S642 in the presence of the SRKR exon as a novel means for reducing BK activation during an AP stimulus.

The functional significance of SRKR inclusion in BK transcripts parallels the known physiological role for BK currents in regulating neural activity in the SCN. BK currents primarily regulate firing frequency at night in SCN neurons, correlating with the window of higher total BK channel expression and larger BK currents in wild-type SCNs (Panda et al., 2002; Meredith et al., 2006; Montgomery et al., 2013). Yet BK currents have little impact on firing rate during the day, despite the presence of a baseline BK current during this time in wild-type SCN neurons (Meredith et al., 2006; Pitts et al., 2006). Our data suggest that part of the reduced influence for BK currents on SCN neuronal activity during the day could be mediated by an increase in SRKR-containing transcripts, leading to decreased AP-induced BK currents.

To further understand how the changes in BK_{SRKR} current properties lead to a reduction in AP-induced current, we considered the effect of SRKR on both kinetic and steady-state parameters, finding alterations in both compared with BK_0. Mutation of S642 to alanine (BK_{SRKR}-S642A) converted BK_{SRKR} steady-state and kinetic properties to be more "BK_0-like" (Fig. 3, C–F). However, the reduction in BK_{SRKR} current compared with BK_0 was eliminated when a step command to the same peak voltage applied during the AP command was used (Fig. 4 G), suggesting that the reduced BK_{SRKR} current elicited by APs may be largely based on kinetic differences between the variants. Consistent with this, BK_{SRKR} currents exhibited slowed activation and faster deactivation at high Ca^{2+} (Fig. 2), factors that could be expected to prominently reduce BK_{SRKR} current activation in response to a brief AP stimulus compared with BK_0. Interestingly, when β4 was coexpressed, which further slows both activation and deactivation of BK_{SRKR}, only the night AP recapitulated the significant difference in peak current between the variants (Fig. 6). In this case, the slower rise time of the night AP compared with the day AP (Fig. 4 A) may facilitate expression of the intrinsic difference between BK_0 and BK_{SRKR}. Collectively, these data strongly support the idea that the expression of BK_0 and BK_{SRKR} is expected to impact excitability in vivo.

Variants with and without the SRKR insert have been previously cloned from human, chick, and turtle tissues (Tseng-Crank et al., 1994; Rosenblatt et al., 1997; Jones et al., 1999). The suppressive effect of SRKR on BK currents in this study is consistent with some data from more limited investigations of the SRKR insert. In the human BK variants, SRKR right-shifted the $V_{1/2}$ of ∼10 mV at 2.4, 75, and 405 µM Ca^{2+} (Tseng-Crank et al., 1994). In another study, BK variants with and without SRKR isolated from the chick cochlea showed no significant differences in $V_{1/2}$ values, but the SRKR-containing clone had reduced voltage sensitivity, indicated by a shallower G-V curve (Rosenblatt et al., 1997). In turtle cochlear variants, the presence of SRKR could either speed or slow activation and left- or right-shift G-V curves, depending on the exons at other splice sites (Jones et al., 1999). Comparing these data to our results, we observed larger $V_{1/2}$ right-shifts of 20–40 mV and no effect on the G-V slope. These differences may be attributable to the novel combination of exons contained within BK_0 and BK_{SRKR} splice variants that may interact to modulate the functional effects of SRKR. For example, the human variant also contained the STREX insert, the chick variant contained an additional eight-residue insert in the RCK1 domain, and both lacked the 27-residue Ca^{2+}-bowl insert at splice site 3 (Tseng-Crank et al., 1994; Rosenblatt et al., 1997). In our study, the addition of the Ca^{2+}-bowl exon also right-shifted the $V_{1/2}$ (Fig. S2). This exon is present in both BK_0 and BK_{SRKR} variants and may enhance the right-shifting effect of SRKR in BK_{SRKR}. Such functional interactions between alternative exons have been described previously in BK channels cloned from *Caenorhabditis elegans* (Johnson et al., 2011). For example, insertions at a splice site within the RCK1 domain can modulate Ca^{2+} sensitivity and activation kinetics, but only when insertions are present at further splice sites within the RCK1–RCK2 linker (Johnson et al., 2011).

Mechanistically, how does inclusion of the SRKR exon regulate phosphorylation? Consistent with our results showing that the dephosphorylation-dependent functional differences at S642 cannot be detected without SRKR present, insertion of SRKR likely alters the

structure of the local protein environment to render S642 susceptible to phosphorylation. Examination of the available crystal structures of BK channels supports this idea (Fig. S4). The structure of the cytosolic domain of a human BK channel variant (Wu et al., 2010) contains the homologous residue to S642 but lacks the SRKR insert. In this structure, S642 is positioned at the extreme N terminus of a β strand immediately after a short five-residue loop toward the C-terminal end of the RCK1 domain. The only other isoform for which there is a crystal structure is a zebrafish isoform that contains the SRKR insert (Yuan et al., 2012). In this structure, the atomic coordinates corresponding to S642 and several surrounding residues, including the SR portion of SRKR, were not obtained. However, the structure suggests that S642 resides within an inter β-strand loop; therefore, the presence of SRKR shifts S642 from within a β-strand region to a loop (Fig. S4). The shift of S642 into this loop could better position it for accessibility to kinases for phosphorylation. In addition, SRKR insertion would distance S642 from the subsequent hydrophobic residues ILI, the proximity of which reduces the predicted phosphorylation score in NetPhos 2.0. Interestingly, of the 30 phospho-residues detected in rat brain lysates (Yan et al., 2008), no peptide fragment containing S642 was detected at all (phosphorylated or not), presumably because of its small size, leaving open the investigation for BK_{SRKR} variants phosphorylated at S642 in native tissues.

How might SRKR and a phosphate group at S642 act to reduce channel activity? In other studies, phosphorylation has been shown to either increase or decrease BK channel activity, depending on the kinase, residue position, and channel variant (Reinhart et al., 1991; Ling et al., 2000; Tian et al., 2001; Yan et al., 2008). In the case of S642 and SRKR, these residues are not located in the vicinity of any of the divalent ion-binding sites, nor are they close to the transmembrane regions that form the voltage sensors or the pore. In the absence of Ca^{2+}, the rightward $V_{1/2}$ shift of BK_{SRKR} compared with BK_0 indicates that phosphorylation of S642 reduces BK channel activation via steps that are Ca^{2+} independent, for example, those involved in intrinsic pore opening or the coupling of voltage-sensor movement to pore opening. However, direct effects on voltage-sensor movement are unlikely caused by the parallel slopes of the G-V curves, which indicate similar voltage sensitivities of activation.

In the presence of Ca^{2+}, SRKR also decreases channel activity, at 1 and 100 µM, but not at 10 µM Ca^{2+}. Thus, as well as the Ca^{2+}-independent effect described above, SRKR also has Ca^{2+}-dependent effects. Changes in several of the many parameters that define Ca^{2+}- and voltage-dependent gating could underlie these effects. Although the precise mechanism is not addressed in the experiments performed in this study, one potential explanation may be that BK_{SRKR} gating is more sensitive to Ca^{2+} than BK_0 gating. Supporting this idea, the decrease in $V_{1/2}$ with increasing Ca^{2+} is greater for BK_{SRKR} compared with BK_0. From zero Ca^{2+}, the $V_{1/2}$ shifts are 45, 188, and 241 mV for BK_{SRKR}, compared with 29, 142, and 211 mV for BK_0 at 1, 10, and 100 µM Ca^{2+} (Fig. 2 C and Table S1). Therefore, SRKR would be expected to inhibit gating via a Ca^{2+}-independent mechanism but conversely increase the ability of Ca^{2+} to gate the channel. At 10 µM Ca^{2+}, the lack of difference in the $V_{1/2}$ of BK_{SRKR} compared with BK_0 could be explained if the enhanced Ca^{2+}-dependent gating overrode the decreased Ca^{2+}-independent gating of BK_{SRKR}. This possibility is suggested by the observation that the range where no differences were observed in the $V_{1/2}$ between BK_0 and BK_{SRKR} (>1 and <100 µM) is near the Ca^{2+} affinities estimated for both the RCK1 and the Ca^{2+}-bowl sites (~4 µM; Bao et al., 2002). Thus, under conditions where the differences in the ability of Ca^{2+} to gate the two variants are expected to be small (in the absence, at low, and at saturating Ca^{2+}), the suppressive effect of SRKR would prevail, while the balance between the two gating processes would be altered at intermediate Ca^{2+} (10 µM).

In addition to the complex effects resulting from the addition of the SRKR exon, we found that coexpression of the predominant brain BK channel accessory subunit, β4, had a range of effects on BK_0 and BK_{SRKR}. As has been reported previously for other BK channel isoforms, β4 slowed both activation and deactivation kinetics (Behrens et al., 2000; Brenner et al., 2000a). In addition, β4 altered BK_0 and BK_{SRKR} G-V relationships in a Ca^{2+}-dependent manner. Ca^{2+}-dependent changes in β4 effects have been observed previously for other BK channel variants (Brenner et al., 2000a, Lippiat et al., 2003; Ha et al., 2004; Wang et al., 2006, 2009; Petrik and Brenner, 2007). At low Ca^{2+}, β4 inhibits BK currents, whereas at high Ca^{2+}, it increases BK currents. A qualitatively similar process is occurring with BK_0 and BK_{SRKR}, with a large rightward shift in G-V curves at 10 µM Ca^{2+} and small rightward (BK_{SRKR}) or leftward (BK_0) shifts at 100 µM Ca^{2+}. Previous work has shown that β4 acts to decrease channel activation by increasing the energetic barrier for intrinsic pore opening and decreasing coupling between the voltage sensors and Ca^{2+} binding, and conversely, β4 acts to increase channel activation by increasing the coupling between Ca^{2+} binding and pore opening, and stabilizing voltage-sensor activation (Wang et al., 2006; Contreras et al., 2012). Given the broadly similar relationships between $V_{1/2}$ changes and Ca^{2+} from previous work and our data, it is reasonable to think that β4 is impacting BK_0 and BK_{SRKR} function via the same mechanisms, with the differences between the variants attributable to shifts in the Ca^{2+} concentration at which β4 switches its net effect on the G-V relationship. This Ca^{2+} concentration would be expected to be higher for BK_{SRKR} than BK_0. However, the

relative interaction of β4's effects on Ca^{2+} dependence, activation, and deactivation kinetics remains to be determined for the observed differences between BK_0 and BK_{SRKR} AP-induced currents.

We wish to thank Hyunjin Choi for assistance with cloning BK splice variants, Jessica Lu for assistance with GenBank sequence submissions, and Man-Kyo Chung for comments on the manuscript.

This work was supported by grants from National Heart, Lung, and Blood Institute (R01-HL102758), National Institute of Diabetes and Digestive Kidney Diseases (R21-DK089337), National Science Foundation (IOS-0956237), and The American Physiological Society's Ryuji Ueno award, sponsored by the S&R Foundation (all to A.L. Meredith). J.P. Whitt was supported by National Institute of Arthritis and Musculoskeletal and Skin Diseases training grant T32-AR007592. All authors declare no conflict of interest.

Sharona E. Gordon served as editor.

Submitted: 31 July 2013
Accepted: 11 October 2013

REFERENCES

Bao, L., A.M. Rapin, E.C. Holmstrand, and D.H. Cox. 2002. Elimination of the BK_{Ca} channel's high-affinity Ca^{2+} sensitivity. *J. Gen. Physiol.* 120:173–189. http://dx.doi.org/10.1085/jgp.20028627

Behrens, R., A. Nolting, F. Reimann, M. Schwarz, R. Waldschütz, and O. Pongs. 2000. hKCNMB3 and hKCNMB4, cloning and characterization of two members of the large-conductance calcium-activated potassium channel β subunit family. *FEBS Lett.* 474:99–106. http://dx.doi.org/10.1016/S0014-5793(00)01584-2

Blom, N., S. Gammeltoft, and S. Brunak. 1999. Sequence and structure-based prediction of eukaryotic protein phosphorylation sites. *J. Mol. Biol.* 294:1351–1362. http://dx.doi.org/10.1006/jmbi.1999.3310

Brayden, J.E., and M.T. Nelson. 1992. Regulation of arterial tone by activation of calcium-dependent potassium channels. *Science.* 256:532–535. http://dx.doi.org/10.1126/science.1373909

Brenner, R., T.J. Jegla, A. Wickenden, Y. Liu, and R.W. Aldrich. 2000a. Cloning and functional characterization of novel large conductance calcium-activated potassium channel β subunits, hKCNMB3 and hKCNMB4. *J. Biol. Chem.* 275:6453–6461. http://dx.doi.org/10.1074/jbc.275.9.6453

Brenner, R., G.J. Peréz, A.D. Bonev, D.M. Eckman, J.C. Kosek, S.W. Wiler, A.J. Patterson, M.T. Nelson, and R.W. Aldrich. 2000b. Vasoregulation by the β1 subunit of the calcium-activated potassium channel. *Nature.* 407:870–876. http://dx.doi.org/10.1038/35038011

Butler, A., S. Tsunoda, D.P. McCobb, A. Wei, and L. Salkoff. 1993. mSlo, a complex mouse gene encoding "maxi" calcium-activated potassium channels. *Science.* 261:221–224. http://dx.doi.org/10.1126/science.7687074

Chen, L., L. Tian, S.H. MacDonald, H. McClafferty, M.S. Hammond, J.M. Huibant, P. Ruth, H.G. Knaus, and M.J. Shipston. 2005. Functionally diverse complement of large conductance calcium- and voltage-activated potassium channel (BK) α-subunits generated from a single site of splicing. *J. Biol. Chem.* 280:33599–33609. http://dx.doi.org/10.1074/jbc.M505383200

Colwell, C.S. 2011. Linking neural activity and molecular oscillations in the SCN. *Nat. Rev. Neurosci.* 12:553–569. http://dx.doi.org/10.1038/nrn3086

Contreras, G.F., A. Neely, O. Alvarez, C. Gonzalez, and R. Latorre. 2012. Modulation of BK channel voltage gating by different auxiliary β subunits. *Proc. Natl. Acad. Sci. USA.* 109:18991–18996. http://dx.doi.org/10.1073/pnas.1216953109

Fakler, B., and J.P. Adelman. 2008. Control of K_{Ca} channels by calcium nano/microdomains. *Neuron.* 59:873–881. http://dx.doi.org/10.1016/j.neuron.2008.09.001

Fuchs, P.A., and M.G. Evans. 1990. Potassium currents in hair cells isolated from the cochlea of the chick. *J. Physiol.* 429:529–551.

Ha, T.S., S.Y. Jeong, S.-W. Cho, H. Jeon, G.S. Roh, W.S. Choi, and C.-S. Park. 2000. Functional characteristics of two BK_{Ca} channel variants differentially expressed in rat brain tissues. *Eur. J. Biochem.* 267:910–918. http://dx.doi.org/10.1046/j.1432-1327.2000.01076.x

Ha, T.S., M.S. Heo, and C.S. Park. 2004. Functional effects of auxiliary β4-subunit on rat large-conductance Ca^{2+}-activated K^+ channel. *Biophys. J.* 86:2871–2882. http://dx.doi.org/10.1016/S0006-3495(04)74339-8

Hu, H., L.R. Shao, S. Chavoshy, N. Gu, M. Trieb, R. Behrens, P. Laake, O. Pongs, H.G. Knaus, O.P. Ottersen, and J.F. Storm. 2001. Presynaptic Ca^{2+}-activated K^+ channels in glutamatergic hippocampal terminals and their role in spike repolarization and regulation of transmitter release. *J. Neurosci.* 21:9585–9597.

Imlach, W.L., S.C. Finch, J.H. Miller, A.L. Meredith, and J.E. Dalziel. 2010. A role for BK channels in heart rate regulation in rodents. *PLoS ONE.* 5:e8698. http://dx.doi.org/10.1371/journal.pone.0008698

Johnson, B.E., D.A. Glauser, E.S. Dan-Glauser, D.B. Halling, R.W. Aldrich, and M.B. Goodman. 2011. Alternatively spliced domains interact to regulate BK potassium channel gating. *Proc. Natl. Acad. Sci. USA.* 108:20784–20789. http://dx.doi.org/10.1073/pnas.1116795108

Jones, E.M.C., M. Gray-Keller, and R. Fettiplace. 1999. The role of Ca^{2+}-activated K^+ channel spliced variants in the tonotopic organization of the turtle cochlea. *J. Physiol.* 518:653–665. http://dx.doi.org/10.1111/j.1469-7793.1999.0653p.x

Kim, E.Y., K.-J. Choi, and S.E. Dryer. 2008. Nephrin binds to the COOH terminus of a large-conductance Ca^{2+}-activated K^+ channel isoform and regulates its expression on the cell surface. *Am. J. Physiol. Renal Physiol.* 295:F235–F246. http://dx.doi.org/10.1152/ajprenal.00140.2008

Ling, S., G. Woronuk, L. Sy, S. Lev, and A.P. Braun. 2000. Enhanced activity of a large conductance, calcium-sensitive K^+ channel in the presence of *Src* tyrosine kinase. *J. Biol. Chem.* 275:30683–30689. http://dx.doi.org/10.1074/jbc.M004292200

Lippiat, J.D., N.B. Standen, I.D. Harrow, S.C. Phillips, and N.W. Davies. 2003. Properties of BK_{Ca} channels formed by bicistronic expression of *hSloα* and β1-4 subunits in HEK293 cells. *J. Membr. Biol.* 192:141–148. http://dx.doi.org/10.1007/s00232-002-1070-0

Livak, K.J., and T.D. Schmittgen. 2001. Analysis of relative gene expression data using real-time quantitative PCR and the $2^{-\Delta\Delta C(T)}$ method. *Methods.* 25:402–408. http://dx.doi.org/10.1006/meth.2001.1262

Meredith, A.L., K.S. Thorneloe, M.E. Werner, M.T. Nelson, and R.W. Aldrich. 2004. Overactive bladder and incontinence in the absence of the BK large conductance Ca^{2+}-activated K^+ channel. *J. Biol. Chem.* 279:36746–36752. http://dx.doi.org/10.1074/jbc.M405621200

Meredith, A.L., S.W. Wiler, B.H. Miller, J.S. Takahashi, A.A. Fodor, N.F. Ruby, and R.W. Aldrich. 2006. BK calcium-activated potassium channels regulate circadian behavioral rhythms and pacemaker output. *Nat. Neurosci.* 9:1041–1049. http://dx.doi.org/10.1038/nn1740

Montgomery, J.R., and A.L. Meredith. 2012. Genetic activation of BK currents in vivo generates bidirectional effects on neuronal excitability. *Proc. Natl. Acad. Sci. USA.* 109:18997–19002. http://dx.doi.org/10.1073/pnas.1205573109

Montgomery, J.R., J.P. Whitt, B.N. Wright, M.H. Lai, and A.L. Meredith. 2013. Mis-expression of the BK K^+ channel disrupts suprachiasmatic nucleus circuit rhythmicity and alters clock-controlled behavior. *Am. J. Physiol. Cell Physiol.* 304:C299–C311. http://dx.doi.org/10.1152/ajpcell.00302.2012

Orio, P., P. Rojas, G. Ferreira, and R. Latorre. 2002. New disguises for an old channel: MaxiK channel β-subunits. *News Physiol. Sci.* 17:156–161.

Panda, S., M.P. Antoch, B.H. Miller, A.I. Su, A.B. Schook, M. Straume, P.G. Schultz, S.A. Kay, J.S. Takahashi, and J.B. Hogenesch. 2002. Coordinated transcription of key pathways in the mouse by the circadian clock. *Cell.* 109:307–320. http://dx.doi.org/10.1016/S0092-8674(02)00722-5

Petersen, O.H., and Y. Maruyama. 1984. Calcium-activated potassium channels and their role in secretion. *Nature.* 307:693–696. http://dx.doi.org/10.1038/307693a0

Petrik, D., and R. Brenner. 2007. Regulation of STREX exon large conductance, calcium-activated potassium channels by the β4 accessory subunit. *Neuroscience.* 149:789–803. http://dx.doi.org/10.1016/j.neuroscience.2007.07.066

Pitts, G.R., H. Ohta, and D.G. McMahon. 2006. Daily rhythmicity of large-conductance Ca^{2+}-activated K^+ currents in suprachiasmatic nucleus neurons. *Brain Res.* 1071:54–62. http://dx.doi.org/10.1016/j.brainres.2005.11.078

Pyott, S.J., A.L. Meredith, A.A. Fodor, A.E. Vázquez, E.N. Yamoah, and R.W. Aldrich. 2007. Cochlear function in mice lacking the BK channel α, β1, or β4 subunits. *J. Biol. Chem.* 282:3312–3324. http://dx.doi.org/10.1074/jbc.M608726200

Reinhart, P.H., S. Chung, B.L. Martin, D.L. Brautigan, and I.B. Levitan. 1991. Modulation of calcium-activated potassium channels from rat brain by protein kinase A and phosphatase 2A. *J. Neurosci.* 11:1627–1635.

Rieg, T., V. Vallon, M. Sausbier, U. Sausbier, B. Kaissling, P. Ruth, and H. Osswald. 2007. The role of the BK channel in potassium homeostasis and flow-induced renal potassium excretion. *Kidney Int.* 72:566–573. http://dx.doi.org/10.1038/sj.ki.5002369

Robitaille, R., and M.P. Charlton. 1992. Presynaptic calcium signals and transmitter release are modulated by calcium-activated potassium channels. *J. Neurosci.* 12:297–305.

Rosenblatt, K.P., Z.P. Sun, S. Heller, and A.J. Hudspeth. 1997. Distribution of Ca^{2+}-activated K^+ channel isoforms along the tonotopic gradient of the chicken's cochlea. *Neuron.* 19:1061–1075. http://dx.doi.org/10.1016/S0896-6273(00)80397-9

Saito, M., C. Nelson, L. Salkoff, and C.J. Lingle. 1997. A cysteine-rich domain defined by a novel exon in a *slo* variant in rat adrenal chromaffin cells and PC12 cells. *J. Biol. Chem.* 272:11710–11717. http://dx.doi.org/10.1074/jbc.272.18.11710

Sausbier, M., H. Hu, C. Arntz, S. Feil, S. Kamm, H. Adelsberger, U. Sausbier, C.A. Sailer, R. Feil, F. Hofmann, et al. 2004. Cerebellar ataxia and Purkinje cell dysfunction caused by Ca^{2+}-activated K^+ channel deficiency. *Proc. Natl. Acad. Sci. USA.* 101:9474–9478. http://dx.doi.org/10.1073/pnas.0401702101

Sausbier, M., C. Arntz, I. Bucurenciu, H. Zhao, X.B. Zhou, U. Sausbier, S. Feil, S. Kamm, K. Essin, C.A. Sailer, et al. 2005. Elevated blood pressure linked to primary hyperaldosteronism and impaired vasodilation in BK channel-deficient mice. *Circulation.* 112:60–68. http://dx.doi.org/10.1161/01.CIR.0000156448.74296.FE

Shen, K.Z., A. Lagrutta, N.W. Davies, N.B. Standen, J.P. Adelman, and R.A. North. 1994. Tetraethylammonium block of Slowpoke calcium-activated potassium channels expressed in Xenopus oocytes: evidence for tetrameric channel formation. *Pflugers Arch.* 426:440–445. http://dx.doi.org/10.1007/BF00388308

Shipston, M.J. 2001. Alternative splicing of potassium channels: a dynamic switch of cellular excitability. *Trends Cell Biol.* 11:353–358. http://dx.doi.org/10.1016/S0962-8924(01)02068-2

Singh, H., R. Lu, J.C. Bopassa, A.L. Meredith, E. Stefani, and L. Toro. 2013. $MitoBK_{Ca}$ is encoded by the *Kcnma1* gene, and a splicing sequence defines its mitochondrial location. *Proc. Natl. Acad. Sci. USA.* 110:10836–10841. http://dx.doi.org/10.1073/pnas.1302028110

Storm, J.F. 1987. Action potential repolarization and a fast after-hyperpolarization in rat hippocampal pyramidal cells. *J. Physiol.* 385:733–759.

Tian, L., R.R. Duncan, M.S. Hammond, L.S. Coghill, H. Wen, R. Rusinova, A.G. Clark, I.B. Levitan, and M.J. Shipston. 2001. Alternative splicing switches potassium channel sensitivity to protein phosphorylation. *J. Biol. Chem.* 276:7717–7720. http://dx.doi.org/10.1074/jbc.C000741200

Tian, L., O. Jeffries, H. McClafferty, A. Molyvdas, I.C.M. Rowe, F. Saleem, L. Chen, J. Greaves, L.H. Chamberlain, H.-G. Knaus, et al. 2008. Palmitoylation gates phosphorylation-dependent regulation of BK potassium channels. *Proc. Natl. Acad. Sci. USA.* 105:21006–21011. http://dx.doi.org/10.1073/pnas.0806700106

Tseng-Crank, J., C.D. Foster, J.D. Krause, R. Mertz, N. Godinot, T.J. DiChiara, and P.H. Reinhart. 1994. Cloning, expression, and distribution of functionally distinct Ca^{2+}-activated K^+ channel isoforms from human brain. *Neuron.* 13:1315–1330. http://dx.doi.org/10.1016/0896-6273(94)90418-9

Wang, B., B.S. Rothberg, and R. Brenner. 2006. Mechanism of β4 subunit modulation of BK channels. *J. Gen. Physiol.* 127:449–465. http://dx.doi.org/10.1085/jgp.200509436

Wang, B., B.S. Rothberg, and R. Brenner. 2009. Mechanism of increased BK channel activation from a channel mutation that causes epilepsy. *J. Gen. Physiol.* 133:283–294. http://dx.doi.org/10.1085/jgp.200810141

Wu, Y., Y. Yang, S. Ye, and Y. Jiang. 2010. Structure of the gating ring from the human large-conductance Ca^{2+}-gated K^+ channel. *Nature.* 466:393–397. http://dx.doi.org/10.1038/nature09252

Xie, J., and D.P. McCobb. 1998. Control of alternative splicing of potassium channels by stress hormones. *Science.* 280:443–446. http://dx.doi.org/10.1126/science.280.5362.443

Yan, J., and R.W. Aldrich. 2012. BK potassium channel modulation by leucine-rich repeat-containing proteins. *Proc. Natl. Acad. Sci. USA.* 109:7917–7922. http://dx.doi.org/10.1073/pnas.1205435109

Yan, J., J.V. Olsen, K.S. Park, W. Li, W. Bildl, U. Schulte, R.W. Aldrich, B. Fakler, and J.S. Trimmer. 2008. Profiling the phospho-status of the BK_{Ca} channel α subunit in rat brain reveals unexpected patterns and complexity. *Mol. Cell. Proteomics.* 7:2188–2198. http://dx.doi.org/10.1074/mcp.M800063-MCP200

Yuan, P., M.D. Leonetti, Y. Hsiung, and R. MacKinnon. 2012. Open structure of the Ca^{2+} gating ring in the high-conductance Ca^{2+}-activated K^+ channel. *Nature.* 481:94–97. http://dx.doi.org/10.1038/nature10670